

The influence of morphology, AGN and environment on the quenching histories of galaxies



Rebecca Jane Smethurst
Pembroke College
University of Oxford

A thesis submitted for the degree of
Doctor of Philosophy
Michaelmas 2016

This thesis is dedicated to
all of those
that dream.

Acknowledgements

Thank ALLL TEH people.

Abstract

GZ shit happens.

Contents

1	Introduction	1
1.1	Galaxy Zoo	3
2	STARPY: A Bayesian analysis of a galaxy's SFH	7
2.1	Star Formation History Models	7
2.2	Probabilistic Fitting Methods	11
2.2.1	Alternative Hierarchical Bayesian approach	19
3	The morphological dependance of quenching	23
3.1	The Red Sample	25
3.2	Green Valley Galaxies	28
3.3	Blue Cloud Galaxies	31
4	The Influence of AGN Feedback	35
4.0.1	Bulgeless galaxies hosting growing black holes	35
5	The influence of the group environment	36
6	Discussion	37
7	Conlusions	38
	Bibliography	39

List of Figures

1.1	GZ2-GALEX sample completeness	4
1.2	Example SDSS images with GZ2 vote fractions	5
2.1	Predicted colours and SFRs of quenching models	8
2.2	SFH models in observational planes	9
2.3	Example STARPY output	13
2.4	Testing STARPY	15
2.5	Comparing complete and look-up table versions of STARPY	16
2.6	Colours of discarded galaxies	18
3.1	SFR-stellar mass plane split by morphology and colour	24
3.2	Population densities of red smooth and disc galaxies	26
3.3	Population densities of green smooth and disc galaxies	29
3.4	Population densities of blue smooth and disc galaxies	32
3.5	Best fit contours for red, green and blue clean galaxies	33

Chapter 1

Introduction

Previous large scale surveys of galaxies have revealed a bimodality in the colour-magnitude diagram (CMD) with two distinct populations; one at relatively low mass, with blue optical colours and another at relatively high mass, with red optical colours (Baldry et al., 2004, 2006; Willmer et al., 2006; Ball et al., 2008; Brammer et al., 2009). These populations were dubbed the ‘blue cloud’ and ‘red sequence’ respectively (Chester & Roberts, 1964; Bower et al., 1992; Driver et al., 2006; Faber et al., 2007). The Galaxy Zoo project (Lintott et al., 2011), which produced morphological classifications for a million galaxies, helped to confirm that this bimodality is not entirely morphology driven (Strateva et al., 2001; Salim et al., 2007; Schawinski et al., 2007; Constantin et al., 2008; Bamford et al., 2009; Skibba et al., 2009), detecting larger fractions of spiral galaxies in the red sequence (Masters et al., 2010) and elliptical galaxies in the blue cloud (Schawinski et al., 2009) than had previously been detected.

The sparsely populated colour space between these two populations, the so-called ‘green valley’, provides clues to the nature and duration of galaxies’ transitions from blue to red. This transition must occur on rapid timescales, otherwise there would be an accumulation of galaxies residing in the green valley, rather than an accumulation in the red sequence as is observed (Arnouts et al., 2007; Martin et al., 2007). Green valley galaxies have therefore long been thought of as the ‘crossroads’ of galaxy evolution, a transition population between the two main galactic stages of the star forming blue cloud and the ‘dead’ red sequence (Bell et al., 2004; Wyder et al., 2007; Schiminovich et al., 2007; Martin et al., 2007; Faber et al., 2007; Mendez et al., 2011;

Gonçalves et al., 2012; Schawinski et al., 2014; Pan et al., 2014).

The intermediate colours of these green valley galaxies have been interpreted as evidence for recent quenching (suppression) of star formation (Salim et al., 2007). Star forming galaxies are observed to lie on a well defined mass-SFR relation, however quenching a galaxy causes it to depart from this relation (Noeske et al. 2007; Peng et al. 2010).

By studying the galaxies which have just left this mass-SFR relation, I can probe the quenching mechanisms by which this occurs. There have been many previous theories for the initial triggers of these quenching mechanisms, including negative feedback from AGN (Di Matteo et al., 2005; Martin et al., 2007; Nandra et al., 2007; Schawinski et al., 2007), mergers (Darg et al., 2010; Cheung et al., 2012; Barro et al., 2013), supernovae winds (Marasco et al., 2012), cluster interactions (Coil et al., 2008; Mendez et al., 2011; Fang et al., 2013) and secular evolution (Masters et al., 2010, 2011; Mendez et al., 2011). By investigating the *amount* of quenching that has occurred in the blue cloud, green valley and red sequence; and by comparing the amount across these three populations, I can apply some constraints to these theories.

The nature of the observed co-evolution of galaxies and their central supermassive black holes (Magorrian et al., 1998; Marconi & Hunt, 2003; Häring & Rix, 2004) and the effects of AGN feedback on galaxies are two of the most important open issues in galaxy evolution. AGN feedback was first suggested as a mechanism for regulating star formation in simulations (Silk & Rees, 1998; Croton et al., 2006; Bower et al., 2006; Somerville et al., 2008) and indirect evidence has been observed for both positive and negative feedback in various systems (see the comprehensive review from Fabian 2012).

The strongest observational evidence for AGN feedback in a population is that the largest fraction of AGN are found in the green valley (Cowie & Barger, 2008; Hickox et al., 2009; Schawinski et al., 2010), suggesting some link between AGN activity and the process of quenching which moves a galaxy from the blue cloud to the red sequence. However, concrete statistical evidence for the effect of AGN feedback on the host galaxy population has so far been elusive.

There are many mechanisms which are proposed to cause quenching; including mergers (Daddi et al., 2010), mass quenching (Kennicutt et al., 1987; Peng et al., 2012), morphological quenching (?) and the environment of a galaxy.

The galaxy environment as a cause of quenching was proposed due to the correlation of both morphology (Dressler, 1980) and the quenched galaxy fraction (?) with environmental density.

BUT does this correlation truly imply causation? Evidence from simulations (?) suggests that the environment may not be the dominant quenching mechanisms for galaxies. Perhaps the correlation of increased galaxy quenched fractions with environment is due to a combination of mergers, mass and morphological quenching. In denser environments, galaxies are more likely to encounter another galaxy in a merger scenario and large viral radii give rise to long infall times during which gas reservoirs can be depleted due to star formation.

To study this I need to look at how quenching timescale changes in groups and clusters of galaxies with different properties in order to isolate the cause of the density-morphology and density-SFR correlations.

1.1 Galaxy Zoo

In this investigation I use visual classifications of galaxy morphologies from the Galaxy Zoo 2¹ citizen science project (Willett et al., 2013), which obtains multiple independent classifications for each galaxy image; the full question tree for each image is shown in Figure 1 of Willett et al. 2013.

The Galaxy Zoo 2 (GZ2) project consists of 304,022 images from the SDSS DR8 (a subset of those classified in Galaxy Zoo 1; GZ1) all classified by *at least* 17 independent users, with the mean number of classifications standing at ~ 42 . The GZ2 sample is more robust than the GZ1 sample and provides more detailed morphological classifications, including features such as bars, the number of spiral arms and the ellipticity of smooth galaxies. It is for these reasons I use the GZ2 sample, as opposed to the GZ1, allowing for further investigation of specific galaxy classes in the future (see Section ??). The only selection that was made on the sample was to remove objects considered to be stars, artefacts or merging pairs by the users (i.e. with $p_{\text{star/artefact}} \geq 0.8$ or $p_{\text{merger}} \geq 0.420$; see Willett et al. 2013 Table 3 and discussion for details of this fractional limit). Further to this, I required NUV photometry

¹<http://zoo2.galaxyzoo.org/>

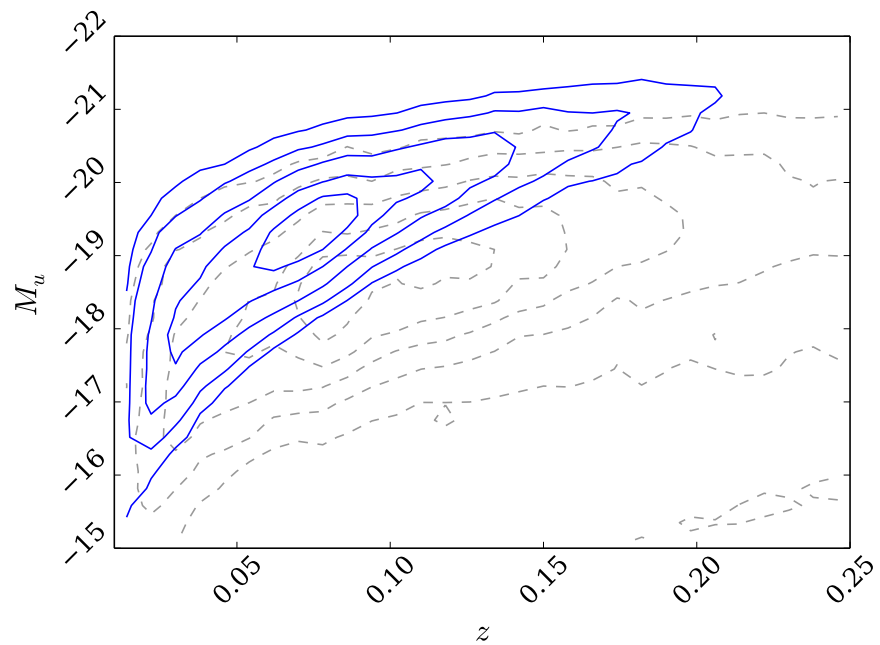


Figure 1.1: Absolute u -band magnitude against redshift for the whole of SDSS (grey dashed lines) in comparison to the GZ2 subsample (blue solid lines). Typical Milky Way L_* galaxies with $M_u \sim -20.5$ are still included in the GZ2 subsample out to the highest redshift of $z \sim 0.25$.

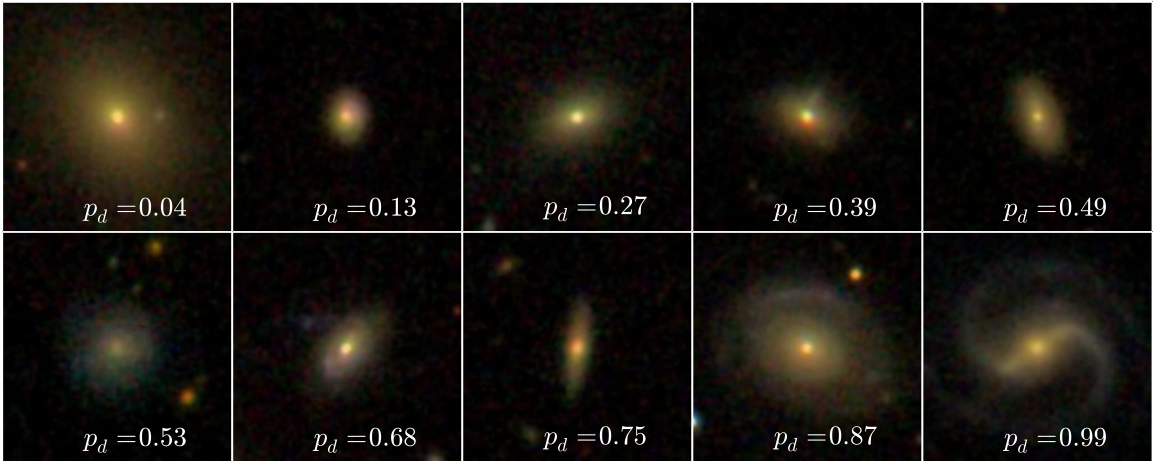


Figure 1.2: Randomly selected SDSS *gri* composite images showing the continuous probabilistic nature of the Galaxy Zoo sample from a redshift range $0.070 < z < 0.075$. The debiased disc vote fraction (see Willett et al. 2013) for each galaxy is shown. The scale for each image is 0.099 arcsec/pixel.

from the GALEX survey, within which $\sim 42\%$ of the GZ2 sample were observed, giving a total sample size of 126,316 galaxies. The completeness of this subsample of GZ2 matched to GALEX is shown in Figure 1.1 with the *u*-band absolute magnitude against redshift for this sample compared with the SDSS data set. Typical Milky Way L_* galaxies with $M_u \sim -20.5$ are still included in the GZ2 subsample out to the highest redshift of $z \sim 0.25$; however dwarf and lower mass galaxies are only detected at the lowest redshifts.

The first task of GZ2 asks users to choose whether a galaxy is mostly smooth, is featured and/or has a disc or is a star/artefact. Unlike other tasks further down in the decision tree, every user who classifies a galaxy image will complete this task (others, such as whether the galaxy has a bar, is dependent on a user having first classified it as a featured galaxy). Therefore I have the most statistically robust classifications at this level.

The classifications from users produces a vote fraction for each galaxy (the debiased fractions calculated by Willett et al. (2013) were used in this investigation); for example if 80 of 100 people thought a galaxy was disc shaped, whereas 20 out of 100 people thought the same galaxy was smooth in shape (i.e. elliptical), that galaxy would have vote fractions $p_s = 0.2$ and $p_d = 0.8$. In this example this galaxy would be included in the ‘clean’ disc sample ($p_d \geq 0.8$) according to Willett et al. (2013)

and would be considered a late-type galaxy. All previous Galaxy Zoo projects have incorporated extensive analysis of volunteer classifications to measure classification accuracy and bias, and compute user weightings (for a detailed description of debiasing and consistency-based user weightings, see either Section 3 of Lintott et al. 2009 or Section 3 of Willett et al. 2013).

The classifications are highly accurate and provide a continuous scale of morphological features, as shown in Figure 1.2, rather than a simple binary classification separating elliptical and disc galaxies. These classifications allow each galaxy to be considered as a probabilistic object with both bulge and disc components.

Chapter 2

STARPY: A Bayesian analysis of a galaxy's SFH

The work in the following chapter has been published in Smethurst et al. (2015).

2.1 Star Formation History Models

The quenched star formation history (SFH) of a galaxy can be simply modelled as an exponentially declining star formation rate (SFR) across cosmic time ($0 \leq t$ [Gyr] ≤ 13.8) as:

$$SFR = \begin{cases} i_{sfr}(t_q) & \text{if } t < t_q \\ i_{sfr}(t_q) \times \exp\left(\frac{-(t-t_q)}{\tau}\right) & \text{if } t > t_q \end{cases} \quad (2.1)$$

where t_q is the onset time of quenching, τ is the timescale over which the quenching occurs and i_{sfr} is an initial constant star formation rate dependent on t_q . A smaller τ value corresponds to a rapid quench, whereas a larger τ value corresponds to a slower quench.

We assume that all galaxies formed at a time $t = 0$ Gyr with an initial burst of star formation. The mass of this initial burst is controlled by the value of the i_{sfr} which is set as the average specific SFR (sSFR) at the time of quenching t_q . Peng et al. (2010) defined a relation (their equation 1) between the average sSFR and redshift (cosmic time, t) by fitting to measurements of the mean sSFR of blue star forming

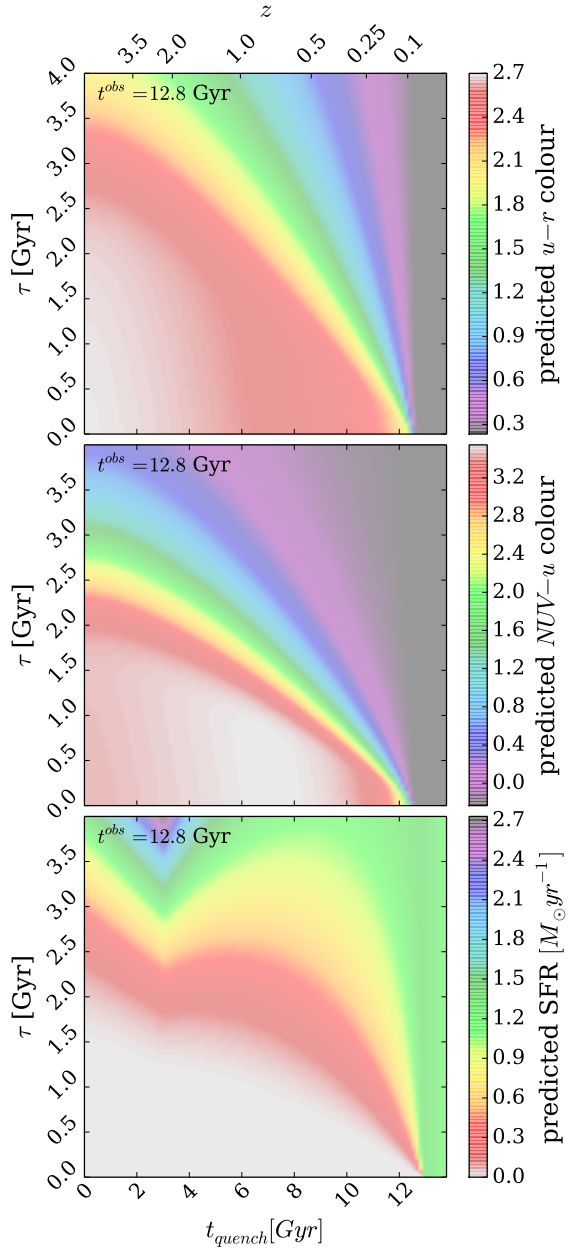


Figure 2.1: Quenching timescale τ versus quenching onset time t in all three panels for the quenched SFH models used in STARPY. Colour shadings show model predictions of the $u - r$ optical colour (top panel), $NUV - u$ colour (middle panel), and star formation rate in $M_{\odot} \text{ yr}^{-1}$ (lower panel), at $t^{\text{obs}} = 12.8 \text{ Gyr}$, the mean observed redshift of the GZ2 sample (see Section 2.1). The combination of optical and NUV colours is a sensitive measure of the $\theta = [t_q, \tau]$ parameter space. Note that all models with $t > 12.8 \text{ Gyr}$ are effectively un-quenched. The ‘kink’ in the bottom panel is due to the assumption that the sSFR is constant prior to $t \sim 3 \text{ Gyr}$ ($z \sim 2.2$).

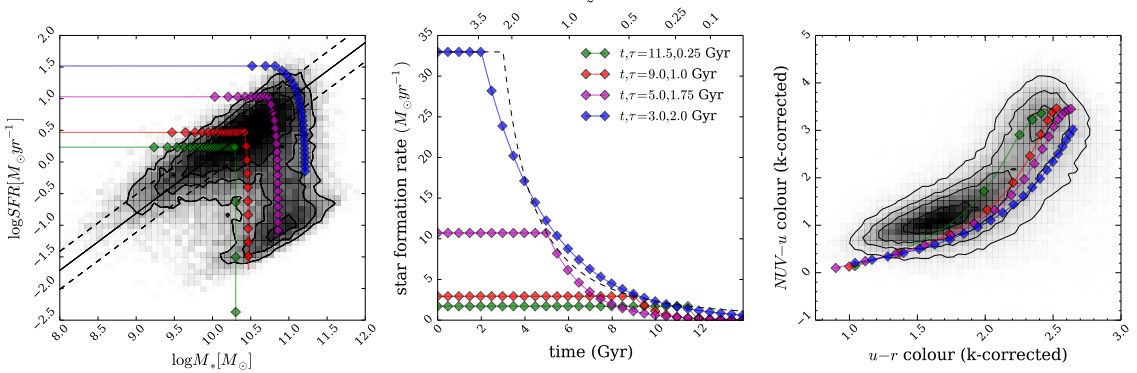


Figure 2.2: Left panel: SFR vs. M_* for all 126,316 galaxies in our full sample (shaded contours), with model galaxy trajectories shown as coloured points/lines with each point representing a time step of 0.5 Gyr. The SFHs of the models are shown in the middle panel, where the SFR is initially constant before quenching at time t and thereafter exponentially declining with a characteristic timescale τ . We set the SFR at the point of quenching to be consistent with the typical SFR of a star-forming galaxy at the quenching time, t (dashed line; Peng et al. 2010). The full range of models reproduces the observed colour-colour properties of the sample (right panel); for clarity the figures show only 4 of the possible models explored in this study. Note that some of the model tracks produce colours redder than the apparent peak of the red sequence in the GZ2 subsample; however this is not the *true* peak of the red sequence due to the necessity for NUV colours from GALEX.

galaxies from SDSS, zCOSMOS and literature values at increasing redshifts (Elbaz et al., 2007; Daddi et al., 2007):

$$sSFR(m, t) = 2.5 \left(\frac{m}{10^{10} M_{\odot}} \right)^{-0.1} \left(\frac{t}{3.5 \text{ Gyr}} \right)^{-2.2} \text{ Gyr}^{-1}. \quad (2.2)$$

Beyond $z \sim 2$ the characteristic SFR flattens and is roughly constant back to $z \sim 6$. The cause for this change is not well understood but can be seen across similar observational data (Peng et al., 2010; González et al., 2010; Béthermin et al., 2012). Motivated by these observations, the relation defined in Peng et al. (2010) is taken up to a cosmic time of $t = 3$ Gyr ($z \sim 2.3$) and prior to this a constant average SFR is assumed (see Figure 2.2). At the point of quenching, t_q , the models are defined to have a SFR which lies on this relationship for the sSFR, for a galaxy with mass, $m = 10^{10.27} M_{\odot}$ (the mean mass of the GZ2 sample; see Section ?? and Figure 2.2).

Under these assumptions the average SFR of our models will result in a lower

value than the relation defined in Peng et al. (2010) at all cosmic times; each galaxy only resides on the ‘main sequence’ at the point of quenching. However galaxies cannot remain on the ‘main sequence’ from early to late times throughout their entire lifetimes given the unphysical stellar masses and SFRs this would result in at the current epoch in the local Universe (Béthermin et al., 2012; Heinis et al., 2014). If we were to include prescriptions for no quenching, starbursts, mergers, AGN etc. into our models we would improve on our reproduction of the average SFR across cosmic time; however we chose to initially focus on the simplest model possible.

Once this evolutionary SFR is obtained, it is convolved with the Bruzual & Charlot (2003) population synthesis models to generate a model SED at each time step. The observed features of galaxy spectra can be modelled using simple stellar population techniques which sum the contributions of individual, coeval, equal-metallicity stars. The accuracy of these predictions depends on the completeness of the input stellar physics. Comprehensive knowledge is therefore required of (i) stellar evolutionary tracks and (ii) the initial mass function (IMF) to synthesise a stellar population accurately.

These stellar population synthesis (SPS) models are an extremely well explored (and often debated) area of astrophysics (Maraston, 2005; Eminian et al., 2008; Conroy et al., 2009; Falkenberg et al., 2009; Chen et al., 2010; Kriek et al., 2010; Miner et al., 2011; Melbourne et al., 2012). In this investigation we chose to utilise the Bruzual & Charlot (2003) *GALEXEV* SPS models, to allow a direct comparison with S14, along with a Chabrier (Chabrier, 2003) IMF, across a large wavelength range ($0.0091 < \lambda [\mu\text{m}] < 160$) with solar metallicity (m62 in the Bruzual & Charlot (2003) models; hereafter BC03).

Fluxes from stars younger than 3 Myr in the SPS model are suppressed to mimic the large optical depth of protostars embedded in dusty formation cloud (as in S14), then filter transmission curves are applied to the fluxes to obtain AB magnitudes and therefore colours. For a particular galaxy at an observed redshift, z , we define the observed time, t^{obs} for that galaxy using the standard cosmological conversion between redshift and time. We utilise the SFH models at this observed time for each individual galaxy to compare the predicted model and observed colours directly.

Figure 2.1 shows these predicted optical and NUV colours at a time of $t^{obs} = 12.8$ Gyr (the average observed time of the Galaxy Zoo 2 sample, $z \sim 0.076$) pro-

vided by the exponential SFH model. These predicted colours will be referred to as $d_{c,p}(t_q, \tau, t^{obs})$, where $c=\{\text{opt}, \text{NUV}\}$ and $p = \text{predicted}$. The SFR at a time of $t^{obs} = 12.8$ Gyr is also shown in Figure 2.1 to compare how this correlates with the predicted colours. The $u-r$ predicted colour shows an immediate correlation with the SFR, however the $NUV - u$ colour is more sensitive to the value of τ and so is ideal for tracing any recent star formation in a population . At small τ (rapid quenching timescales) the $NUV - u$ colour is insensitive to t_q , whereas at large τ (slow quenching timescales) the colour is very sensitive to t_q . Together the two colours are ideal for tracing the effects of t_q and τ in a population.

We stress here that this model is not a fully hydrodynamical simulation, it is a simple model built in order to test the understanding of the evolution of galaxy populations. These models are therefore not expected to accurately determine the SFH of every galaxy in the GZ2 sample, in particular galaxies which have not undergone any quenching. In this case the models described above can only attribute a constant star formation rate to these unquenched galaxies. In reality, there are many possible forms of SFH that a galaxy can take, a few of which have been investigated in previous literature; starbursts (Canalizo & Stockton, 2001), a power law (Glazebrook et al., 2003), single stellar populations (Trager et al., 2000; Sánchez-Blázquez et al., 2006; Vazdekis et al., 2010) and metallicity enrichment (De Lucia et al., 2014). Incorporating these different SFHs along with prescriptions for mergers and a reinvigoration of star formation post quench into our models is a possible future extension to this work once the results of this initial study are well enough understood to permit additional complexity to be added.

2.2 Probabilistic Fitting Methods

In order to achieve robust conclusions we conduct a Bayesian analysis (Sivia & Skilling, 2006; Mackay, 2003) of our SFH models in comparison to the observed GZ2 sample data. This approach requires consideration of all possible combinations of $\theta \equiv (t_q, \tau)$. Assuming that all galaxies formed at $t = 0$ Gyr with an initial burst of star formation, we can assume that the ‘age’ of each galaxy in the GZ2 sample is equivalent to an observed time, t_k^{obs} . We then use this ‘age’ to calculate the predicted model colours at this cosmic time for a given combination of θ : $d_{c,p}(\theta_k, t_k^{obs})$ for both optical and NUV ($c = \text{opt}, \text{NUV}$) colours. We can now directly compare our

model colours with the observed GZ2 galaxy colours, so that for a single galaxy k with optical ($u - r$) colour, $d_{opt,k}$ and NUV ($NUV - u$) colour, $d_{NUV,k}$, the likelihood $P(d_k|\theta_k, t_k^{obs})$ is:

$$P(d_k|\theta_k, t_k^{obs}) = \frac{1}{\sqrt{2\pi\sigma_{opt,k}^2}} \frac{1}{\sqrt{2\pi\sigma_{NUV,k}^2}} \exp \left[-\frac{(d_{opt,k} - d_{opt,p}(\theta_k, t_k^{obs}))^2}{\sigma_{opt,k}^2} \right] \exp \left[-\frac{(d_{NUV,k} - d_{NUV,p}(\theta_k, t_k^{obs}))^2}{\sigma_{NUV,k}^2} \right] \quad (2.3)$$

We have assumed that $P(d_{opt}|\theta_k, t_k^{obs})$ and $P(d_{NUV}|\theta_k, t_k^{obs})$ are independent of each other and that the errors on the observed colours are also independent. To obtain the probability of each combination of θ values given the GZ2 data: $P(\theta_k|d_k, t^{obs})$, i.e. how likely is a single SFH model given the observed colours of a single GZ2 galaxy, we utilise Bayes' theorem:

$$P(\theta_k|d_k, t^{obs}) = \frac{P(d_k|\theta_k, t^{obs})P(\theta_k)}{\int P(d_k|\theta_k, t^{obs})P(\theta_k)d\theta_k}. \quad (2.4)$$

We assume a flat prior on the model parameters so that:

$$P(\theta_k) = \begin{cases} 1 & \text{if } 0 \leq t_q \text{ [Gyr]} \leq 13.8 \text{ and } 0 \leq \tau \text{ [Gyr]} \leq 4 \\ 0 & \text{otherwise.} \end{cases} \quad (2.5)$$

As the denominator of Equation 2.4 is a normalisation factor, comparison between likelihoods for two different SFH models (i.e., two different combinations of $\theta_k = [t_q, \tau]$) is equivalent to a comparison of the numerators. Calculation of $P(\theta_k|d_k, t^{obs})$ for any θ is possible given galaxy data from the GZ2 sample. Markov Chain Monte Carlo (MCMC; Mackay 2003; Foreman-Mackey et al. 2013; Goodman & Weare 2010) provides a robust comparison of the likelihoods between θ values; here we choose *emcee*,¹ a Python implementation of an affine invariant ensemble sampler by Foreman-Mackey et al. (2013).

This method allows for a more efficient exploration of the parameter space by avoiding those areas with low likelihood. A large number of ‘walkers’ are started at an initial position where the likelihood is calculated; from there they individually ‘jump’ to a new area of parameter space. If the likelihood in this new area is greater (less) than the original position then the ‘walkers’ accept (reject) this change in position.

¹[emcee13.iel.fm/emcee/](http://emcee.readthedocs.io)

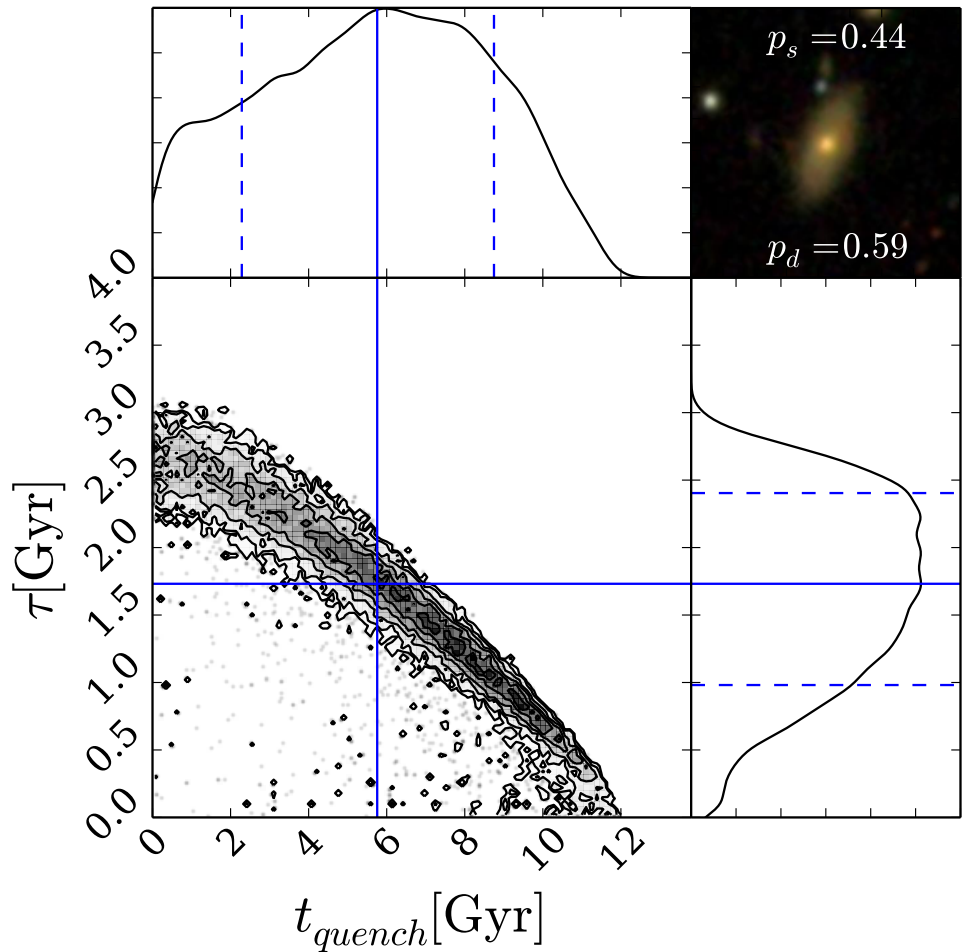


Figure 2.3: Example output from STARPY for a galaxy within the red sequence. The contours show the positions of the ‘walkers’ in the Markov Chain (which are analogous to the areas of high probability) for the quenching models described by $\theta = [t_q, \tau]$ and the histograms show the 1D projection along each axis. Solid (dashed) blue lines show the best fit model (with $\pm 1\sigma$) to the galaxy data. The postage stamp image is shown in the top right along with the debiased vote fractions for smooth (p_s) and disc (p_d) from Galaxy Zoo 2.

Any new position then influences the direction of the ‘jumps’ of other walkers. This is repeated for the defined number of steps after an initial ‘burn-in’ phase. *emcee* returns the positions of these ‘walkers’, which are analogous to the regions of high probability in the model parameter space. The model outlined above has been coded using the *Python* programming language into a package named STARPY which has been made freely available to download². An example output from this Python package for a single galaxy from the GZ2 sample in the red sequence is shown in Figure 2.2. The contours show the positions of the ‘walkers’ in the Markov Chain which are analogous to the areas of high probability.

In order to test that STARPY can find the correct quenching model for a given observed colour, 25 synthesised galaxies were created with known SFHs (i.e. known values of θ) from which optical and NUV colours were generated. These were input into STARPY to ensure that the known values of θ were reproduced, within error, for each of the 25 synthesised galaxies. Figure 2.4 shows the results for each of these 25 synthesised galaxies, with the known values of θ shown by the red lines. In some cases this red line does not coincide with the peak of the distribution shown in the histograms for one parameter, however in all cases the intersection of the red lines is within the sample contours.

We find peaks in the histograms across all areas of the parameter space in both dimensions of $[t, \tau]$, ensuring that any conclusions drawn from these distributions are due to a superposition of extended probability distributions, as opposed to a bimodal distribution of probability distributions across all galaxies.

Considering the size of the sample in this investigation of 126,316 galaxies total, a three dimensional look up table (in observed time, quenching time and quenching rate) was generated using the star formation history function in STARPY to speed up the run time.

We wish to consider the model parameters for the populations of galaxies across the colour magnitude diagram for both smooth and disc galaxies, therefore we run the STARPY package on each galaxy in the GZ2 sample. This was extremely time consuming; for each combination of θ values which *emcee* proposes, a new SFH must be built, prior to convolving it with the BC03 SPS models at the observed age and then predicted colours calculated from the resultant SED. For a single galaxy this

²github.com/zooniverse/starp

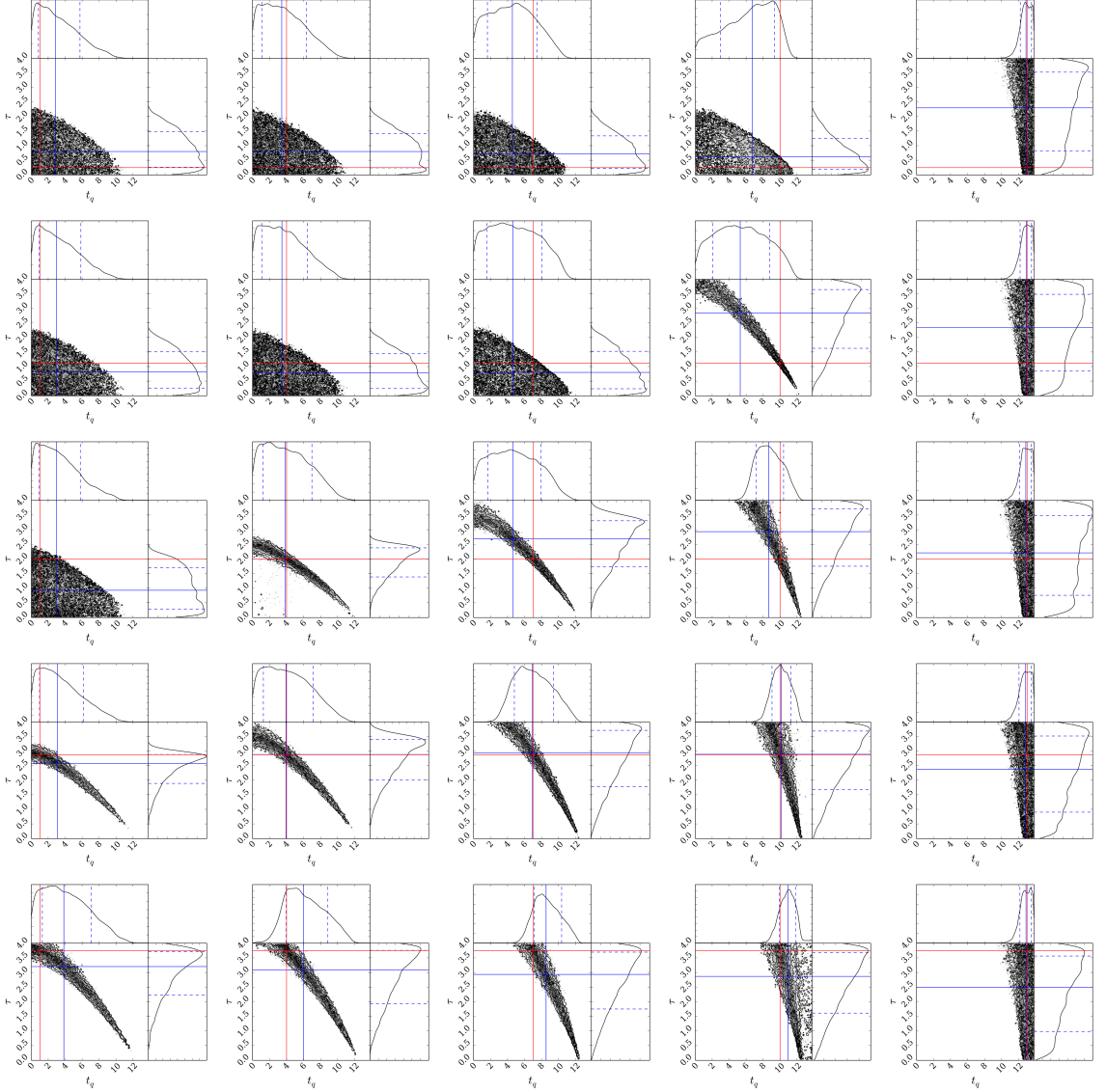


Figure 2.4: Results from STARPY for an array of synthesised galaxies with known, i.e. true, t_q and τ values (marked by the red lines) using the complete function to calculate the predicted colour of a proposed set of θ values in each MCMC iteration, assuming an error on the calculated known colours of $\sigma_{u-r} = 0.124$ and $\sigma_{NUV-u} = 0.215$, the average errors on the GZ sample colours. In each case STARPY succeeds in locating the true parameter values within the degeneracies of the star formation history model.

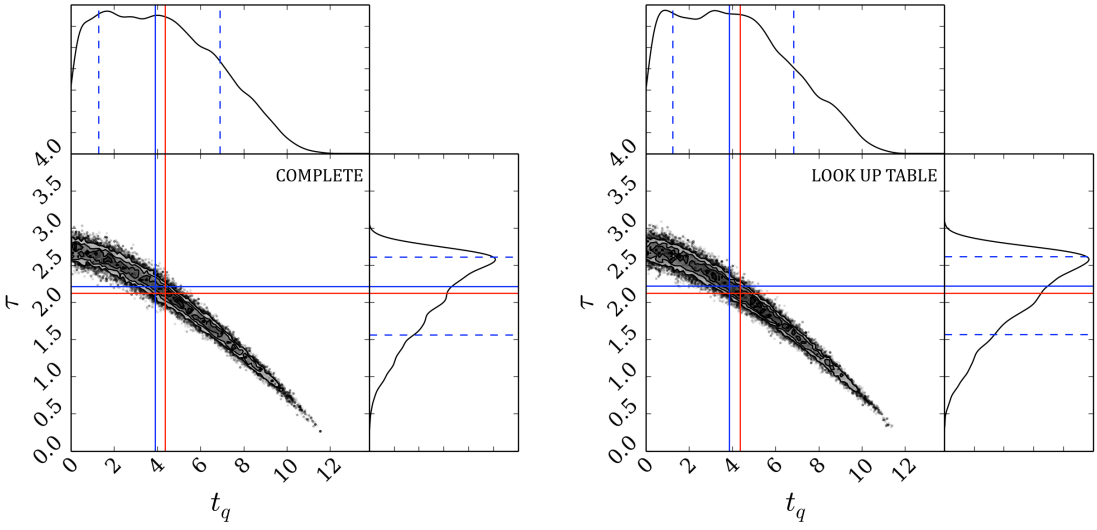


Figure 2.5: Left panel: Results from STARPY for true t_q and τ values (red lines) using the complete function to calculate the predicted colour of a proposed set of θ values in each MCMC iteration. The median walker position (the 50th percentile of the Bayesian probability distribution) is shown by the solid blue line with the dashed lines encompassing 68%($\pm 1\sigma$) of the samples (the 16th and 84th percentile positions). The time taken to run for a single galaxy using this method is approximately 2 hours. Right panel: Results from STARPY for true t_q and τ values using a look up table generated from the complete function to calculate the predicted colour of a proposed set of θ values in each MCMC iteration. The time taken to run for a single galaxy using this method is approximately 2 minutes.

Table 2.1: Median walker positions (the 50th percentile; as shown by the blue solid lines in Figure 2.5) found by STARPY for a single galaxy, using the complete star formation history function and a look up table to speed up the run time. The errors quoted define the region in which 68% of the samples are located, shown by the dashed blue lines in Figure 2.5. The known true values are also quoted, as shown by the red lines in Figure 2.5. All values are quoted to three significant figures.

	t_q	τ
True	4.37	2.12
Complete	$3.893 \pm^{3.014}_{2.622}$	$2.215 \pm^{0.395}_{0.652}$
Look up table	$3.850 \pm^{2.988}_{2.619}$	$2.218 \pm^{0.399}_{0.649}$

Table 2.2: Number of galaxies in each population which had walker positions discarded due to low probability in order to exclude those galaxies from the analysis which were poorly fit by this quenching model.

	Red Sequence	Green Valley	Blue Cloud
All walkers discarded	1420 (7.00%)	437 (2.41%)	3109 (5.37%)
More than half walker positions discarded	2010 (9.92%)	779 (4.30%)	6669 (11.52%)

takes up to 2 hours on a typical desktop machine for long Markov Chains. A look-up table was therefore generated at 50 t^{obs} , for 100 t_{quench} and 100 τ values; this was then interpolated over for a given observed galaxy’s age and proposed θ values at each step in the Markov Chain. This ensures that a single galaxy takes approximately 2 minutes to run on a typical desktop machine. Figure 2.5 shows an example of how using the look up table in place of the full function does not affect the results to a significant level. Table 2.2 quotes the median walker positions (the 50th percentile of the Bayesian probability distribution) along with their $\pm 1\sigma$ ranges for both methods in comparison to the true values specified to test STARPY. The uncertainties incorporated into the quoted values by using the look up table are therefore minimal with a maximum $\Delta = 0.043$.

Using this lookup table, each of the 126,316 total galaxies in the GZ2 sample was run through STARPY on multiple cores of a computer cluster to obtain the Markov Chain positions (analogous to $P(\theta_k|d_k)$) for each galaxy, k (see Figure 2.2). In each case the Markov Chain consisted of 100 ‘walkers’ which took 400 steps in the ‘burn-in’ phase and 400 steps thereafter, at which point the MCMC acceptance fraction was checked to be within the range $0.25 < f_{acc} < 0.5$ (which was true in all cases). Due to the Bayesian nature of this method, a statistical test on the results is not possible; the output is probabilistic in nature across the entirety of the parameter space.

These individual galaxy positions are then combined to visualise the areas of high probability in the model parameter space across a given population (e.g. the green valley).

We discard walker positions returned by STARPY with a corresponding probability of $P(\theta_k|d_k) < 0.2$ in order to exclude galaxies which are not well fit by the quenching

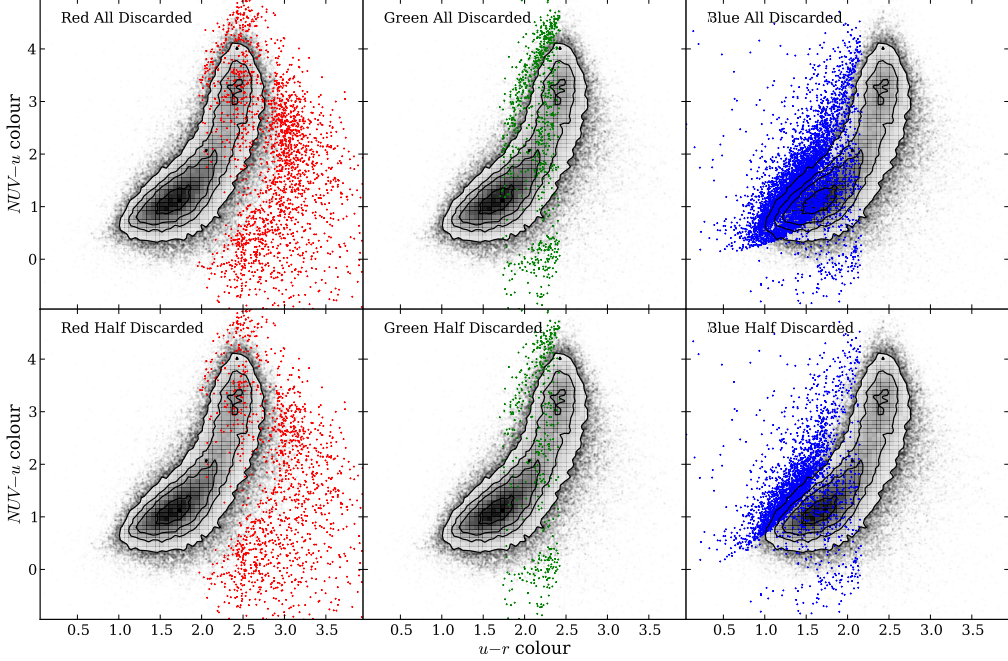


Figure 2.6: Contours show the full GZ2 subsample optical-NUV colour-colour diagram. The points show the positions of the galaxies which had all (top panels) or more than half (bottom panel) of their walker positions discarded due to their low probability for the red sequence (left), green valley (middle) and blue cloud (right).

model; for example blue cloud galaxies which are still star forming will be poorly fit by a quenching model (see Section 2.1). This raises the issue of whether we exclude a significant fraction of our galaxy sample and whether those galaxies reside in a specific location of the colour-magnitude. The fraction of galaxies which had all or more than half of their walker positions discarded due to low probability are shown in Table 2.2. Using this constraint, 2.4%, 7.0% and 5.4% of green, red and blue galaxies respectively had *all* of their walker positions discarded.

This is not a significant fraction of either population, therefore this shows that the STARPY module is effective in fitting the majority of galaxies and that this method of discarding walker positions ensures that poorly fit galaxies are removed from the analysis of the results. Figure 2.6 shows that these galaxies with discarded walker positions are also scattered across the optical-NUV colour-colour diagram and therefore STARPY is also effective in fitting galaxies across this entire plane.

The Markov Chain positions are then binned and weighted by their corresponding logarithmic posterior probability $\log[P(\theta_k | d_k)]$, provided by the *emcee* package,

to further emphasise the features and differences between each population in the visualisation. The GZ2 data also provides uniquely powerful continuous measurements of a galaxy’s morphology, therefore we utilise the user vote fractions to obtain separate model parameter distributions for both smooth and disc galaxies. This is obtained by also weighting by the morphology vote fraction when the binned positions are summed. We stress that this portion of the methodology is a non-Bayesian visualisation of the combined individual galaxy results for each population.

For example, the galaxy shown in Figure 2.2 would contribute almost evenly to both the smooth and disc parameters due to the GZ2 vote fractions. Since galaxies with similar vote fractions contain both a bulge and disc component, this method is effective in incorporating intermediate galaxies which are thought to be crucial to the morphological changes between early- and late-type galaxies. It was the consideration of these intermediate galaxies which was excluded from the investigation by S14.

2.2.1 Alternative Hierarchical Bayesian approach

The approach presented above relies upon a visualisation of the SFHs across each population, with no inference involved beyond the use of STARPY to derive the individual galaxy SFHs. The preferred approach to this problem would be to use a hierarchical Bayesian method to determine the ‘hyper-parameters’ that describe the distribution of the parent population $\theta' = [t'_q, \tau']$ that each individual galaxy’s SFH is drawn from.

We want the posterior PDF for $\vec{\theta}'$ to describe a galaxy population:

$$P(\vec{\theta}'|\vec{d}) = \frac{P(\vec{d}|\vec{\theta}')P(\vec{\theta}')}{P(\vec{d})}, \quad (2.6)$$

where \vec{d} represents all of the optical and NUV colour data in a population $\{\vec{d}_k\}$. For one galaxy, k , the marginalised likelihood is:

$$P(d_k|\vec{\theta}') = \iint P(d_k|t_k, \tau_k)P(t_k, \tau_k|\vec{\theta}') dt_k d\tau_k \quad (2.7)$$

and for all galaxies, N , therefore:

$$P(\vec{d}|\vec{\theta}') = \prod_k^N P(d_k|\vec{\theta}'). \quad (2.8)$$

Using STARPY for individual galaxies we sample from the ‘interim’ posterior $P(t_k, \tau_k | d_k)$ which we can relate to $P(d_k | t_k, \tau_k)$ so that:

$$P(d_k | \vec{\theta}') = \iint P(t_k, \tau_k | d_k) \cdot P(d_k) \cdot \frac{P(t_k, \tau_k | \vec{\theta}')}{P(t_k, \tau_k)} dt_k d\tau_k. \quad (2.9)$$

In order to calculate this we draw N_s random samples, r , from the interim posterior, $P(t_k, \tau_k | d_k)$ so that Equation 2.9 can be expressed as a sum over a number of random samples, N_s (as with the calculation of an expected mean):

$$P(d_k | \vec{\theta}') = \frac{P(d_k)}{N_s} \sum_r^{N_s} \frac{P(t_{k,r}, \tau_{k,r} | \vec{\theta}')}{P(t_k, \tau_k)}, \quad (2.10)$$

for the r^{th} sample of N_s total samples taken from one galaxy’s, k , interim posterior PDF. This fraction is known as the ‘importance weight’, w_r , in importance sampling.

However, we also have two morphological vote fractions that we can weight by to determine separate hyper-parameters, $\vec{\theta}' = [\vec{\theta}_d', \vec{\theta}_s']$, for both disc, d , and smooth, s , galaxies. Therefore:

$$w_r = \frac{P(t_{k,r}, \tau_{k,r} | \vec{\theta}')}{P(t_k, \tau_k)} = \frac{p_{d,k} P(t_{k,r}, \tau_{k,r} | \vec{\theta}_d') + p_{s,k} P(t_{k,r}, \tau_{k,r} | \vec{\theta}_s')}{P(t_k, \tau_k)} \quad (2.11)$$

If we substitute equation 2.10 into equation 2.6 we find that the $P(d_k)$ terms cancel and we are left with:

$$P(\vec{\theta}' | \vec{d}) = P(\vec{\theta}') \prod_k^N \frac{1}{N_{s,k}} \sum_r^{N_s} w_r, \quad (2.12)$$

where $P(\vec{\theta}')$ is the assumed prior on the hyper-parameters, which is assumed to be uniform.

This approach is heavily dependent on what shape is assumed for the hyper-distribution; a decision which is not trivial. It is often common for this function to take the form of a multi-component Gaussian mixture model (Mackay, 2003; Lahav et al., 2000). For example a two component Gaussian mixture model in $[t, \tau]$ space is described by eight hyper-parameters for a single morphology, $\vec{\theta}' = [\mu_{t,1}, \sigma_{t,1}, \mu_{\tau,1}, \sigma_{\tau,1}, \mu_{t,2}, \sigma_{t,2}, \mu_{\tau,2}, \sigma_{\tau,2}]$. Here we also assume no covariance between hyper-parameters for simplicity.

We used this assumption of a two component Gaussian mixture model, to infer the population parameters for both the AGN-HOST and INACTIVE populations and the results are shown in Figure ???. These results were produced by drawing $N_s = 100$ random samples from each galaxy, k , in each mass bin. We plot the distributions for a given morphology by taking the median value of the posterior distribution for each of the 8 parameters describing the two component Gaussian mixture. We can see in Figure ?? that this hierarchical method produces similar distributions for the AGN-HOST and INACTIVE samples. This finding is not expected given the differences between the two samples in colour-colour space seen in Figure ??.

In order to test whether this assumption of a multi-component Gaussian mixture model is appropriate, we sampled the inferred hierarchical distributions to produce replica datasets in optical-NUV colour space. These are shown here in Figure ?? in comparison to the observed colour-colour distributions of the AGN-HOST and INACTIVE samples. For all masses and morphologies the replicated $u - r$ and $NUV - u$ colours do not accurately match the observed data.

We also varied the value of N_s and found that increasing the number of samples drawn did not improve this fit for either the AGN-HOST or INACTIVE populations. Similarly increasing the number of components in the Gaussian mixture model did not immediately improve the accuracy of the fit. We therefore concluded that this functional form of the population distribution was unsatisfactory.

The approach described in section 2.2 and applied throughout the rest of this work was motivated by the investigation increasing the number of samples, N_s drawn from the posterior of each galaxy, k , until the point where all the samples were drawn. Instead of attempting to infer parameters to describe this distribution, as above, we presented the distribution itself. The distributions produced by this visualisation method, shown in Figures ?? and ??, reveal the complexity that the parent distribution must describe which, as we concluded earlier, cannot be effectively modelled.

We also tested whether this method is reasonable by producing replica datasets in optical-NUV colour space, as before, by drawing 1000 $[t, \tau]$ values from the unweighted summed distributions presented in Figures ?? and ???. These replica datasets are shown here in Figure ?? in comparison to the observed colour-colour distributions of the AGN-HOST and INACTIVE samples. Comparing these replica colours in Figure ??, with those produced by drawing from the inferred hierarchical distributions, shown

in Figure ??, we can see that they produce a more accurate match to the observed data for the majority of masses and morphologies.

We therefore use this visualisation method to display the parent population distribution, rather than quoting inferred values to describe it.

Chapter 3

The morphological dependance of quenching

The work in the following chapter has been published in Smethurst et al. (2015).

Figure 3.1 shows the SFR versus the stellar mass for the observed GZ2 sample which has been split into blue cloud, green valley and red sequence populations as well as into the ‘clean’ disc and smooth galaxy samples (with GZ2 vote fractions of $p_d \geq 0.8$ and $p_s \geq 0.8$ respectively). The green valley galaxies are indeed a population which have either left, or begun to leave, the star forming sequence or have some residual star formation still occurring.

The left panel in Figure 2.2 shows a handful of quenching models and how they reproduce the observed relationship between the SFR and the mass of a galaxy, including how at the time of quenching they reside on the star forming sequence shown by the solid black line for a galaxy of mass, $M = 10^{10.27} M_\odot$. The right panel shows how these SFRs translate into the optical-NUV colour-colour plane to reproduce observed colours of green valley and red sequence galaxies. Some of the SFHs produce colours redder than the apparent peak of the red sequence in the GZ2 subsample; however this is not the *true* peak of the red sequence due to the necessity for NUV colours from GALEX (see Section 1.1).

The majority of the red galaxies in the sample therefore lie towards the *blue end* of the red sequence and have a small amount of residual star formation in order to be detected in the NUV resulting in a specific subset of the red sequence studied in this

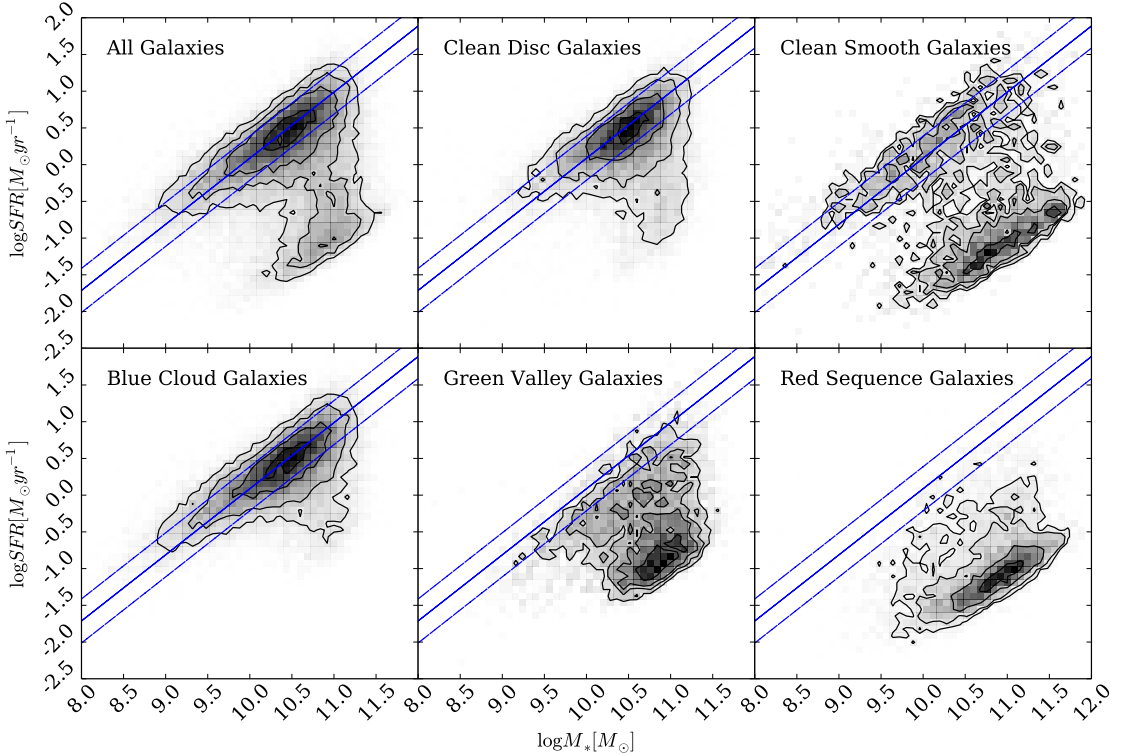


Figure 3.1: Star formation rate versus stellar mass diagrams show the different populations of galaxies (top row, left to right: all galaxies, GZ2 ‘clean’ disc and smooth galaxies; bottom row, left to right: blue cloud, green valley and red sequence galaxies) and how they contribute to the star forming sequence (from Peng et al. (2010), shown by the solid blue line with 0.3 dex scatter by the dashed lines). Based on positions in these diagrams, the green valley does appear to be a transitional population between the blue cloud and the red sequence. Detailed analysis of star formation histories can elucidate the nature of the different populations’ pathways through the green valley. The clean smooth and disc samples are described in Section 1.1.

investigation. Only 47% of the red sequence galaxies present in the entire Galaxy Zoo 2 sample are matched with GALEX to produce our final sample of 126,316 galaxies, as opposed to 72% of the blue cloud and 53% of the green valley galaxies. This limitation should be taken into account when considering the results in the following sections.

The SFH models were implemented with the STARPY package to produce Figures 3.2, 3.3 & 3.4 for the red sequence, green valley and blue cloud populations of smooth and disc galaxies respectively. The percentages shown in Figures 3.2, 3.3 & 3.4 are calculated as the fractions of the combined posterior probability distribution located in each region of parameter space for a given population.

Since the sample contains such a large number of galaxies, we interpret these fractions as broadly equivalent to the percentage of galaxies in a given population undergoing quenching within the stated timescale range. Although this is not quantitatively exact, it is nevertheless a useful framework for interpreting the results of combining the individual posterior probability distributions of each galaxy.

Also shown in Figure 11 are the median walker positions (the 50th percentile of the Bayesian probability distribution) of each individual galaxy, split into red, green and blue populations also with a hard cut in the vote fraction of $p_d > 0.5$ and $p_s > 0.5$ to show the disc and smooth populations respectively. These positions were calculated without discarding any walker positions due to low probability and without weighting by vote fractions; therefore this may be more intuitive to understand than Figures 3.2, 3.3 & 3.4.

Although the quenching timescales are continuous in nature, in this Section we refer to rapid, intermediate and slow quenching timescales which correspond to ranges of τ [Gyr] < 1.0 , $1.0 < \tau$ [Gyr] < 2.0 and τ [Gyr] > 2.0 respectively for ease of discussion.

3.1 The Red Sample

The left panel of Figure 3.2 reveals that smooth galaxies with red optical colours show a preference (49.5%; see Figure 3.2) for rapid quenching timescales across all cosmic time resulting in a very low current SFR. For these smooth red galaxies we

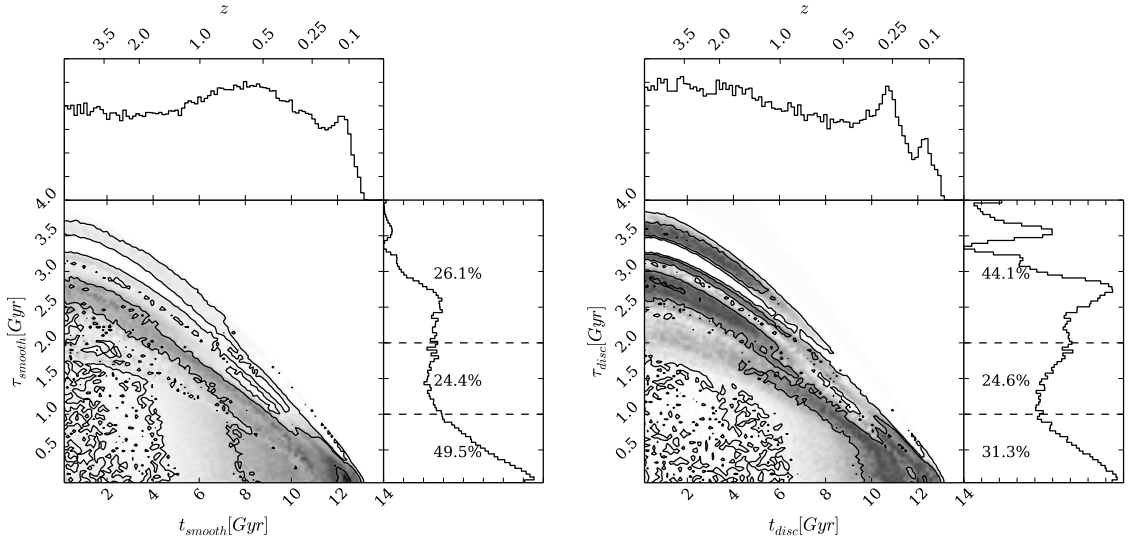


Figure 3.2: Contour plots showing the combined positions in the Markov Chain for all red galaxies in this study, weighted by the logarithmic probability of each position (see Section 2.2) and also by the morphological vote fractions from GZ2 to give the areas of high probability in the model parameter space for both bulge (left) and disc (right) dominated systems. The histograms show the projection into one dimension for each parameter. The dashed lines show the separation between rapid ($\tau [\text{Gyr}] < 1.0$), intermediate ($1.0 < \tau [\text{Gyr}] < 2.0$) and slow ($\tau [\text{Gyr}] > 2.0$) quenching timescales with the fraction of the combined posterior probability distribution in each region shown (see Section 2.2).

see, at early times only, a preference for slow and intermediate timescales in the left panel of Figure 3.2. Perhaps this is the influence of intermediate galaxies (with $p_s \sim p_d \sim 0.5$), hence why similar high probability areas exist for both the smooth-like and disc-like galaxies in the left and right panels of Figure 3.2. This is especially apparent considering there are far more of these intermediate galaxies than those that are definitively early- or late-types (see Table ??). These galaxies are those whose morphology cannot be easily distinguished either because they are at a large distance or because they are an S0 galaxy whose morphology can be interpreted by different users in different ways. Willett et al. (2013) find that S0 galaxies expertly classified by Nair & Abraham (2010) are more commonly classified as ellipticals by GZ2 users, but have a significant tail to high disc vote fractions, giving a possible explanation as to the origin of this area of probability.

The right panel of Figure 3.2 reveals that red disc galaxies show similar preferences for rapid (31.3%) and slow (44.1%) quenching timescales. The preference for *very* slow ($\tau > 3.0$ Gyr) quenching timescales (which are not seen in either the green valley or blue cloud, see Figures 3.3 and 3.4) suggests that these galaxies have only just reached the red sequence after a very slow evolution across the colour-magnitude diagram. Considering their limited number and our requirement for NUV emission, it is likely that these galaxies are currently on the edge of the red sequence having recently (and finally) moved out of the green valley. Table ?? shows that 3.9% of our sample are red sequence clean disc galaxies, i.e. red late-type spirals. This is, within uncertainties, in agreement with the findings of Masters et al. (2010), who find $\sim 6\%$ of late-type spirals are red when defined by a cut in the $g - r$ optical colour (rather than with $u - r$ as implemented in this investigation) and are at the ‘blue end of the red sequence’.

Despite the dominance of slow quenching timescales, the red disc galaxies also show some preference for rapid quenching timescales (31.3%), similar to the red smooth galaxies but with a lower probability. Perhaps these rapid quenching timescales can also be attributed to a morphological change, suggesting that the quenching has occurred more rapidly than the morphological change to a bulge dominated system.

Comparing the resultant SFRs for both the smooth- and disc-like galaxies in Figure 3.2 by noticing where the areas of high probability lie with respect to the bottom panel of Figure 2.1 (which shows the predicted SFR at an observation time of $t \sim 12.8$ Gyr, the average ‘observed’ time of the GZ2 population) reveals that

red disc galaxies with a preference for slow quenching still have some residual star formation occurring, $\text{SFR} \sim 0.105 M_{\odot} \text{yr}^{-1}$, whereas the smooth galaxies with a dominant preference for rapid quenching have a resultant $\text{SFR} \sim 0.0075 M_{\odot} \text{yr}^{-1}$. This is approximately 14 times less than the residual SFR still occurring in the red sequence disc galaxies. Within error, this is in agreement with the findings of Tojeiro et al. (2013) who, by using the VErsatile SPectral Analyses spectral fitting code (VESPA; Tojeiro et al. 2007), found that red late-type spirals show 17 times more recent star formation than red elliptical galaxies.

These results for the red galaxies investigated here with NUV emission, have many implications for green valley galaxies, as all of these systems must have passed through the green valley on their way to the red sequence.

3.2 Green Valley Galaxies

In Figure 3.3 we can make similar comparisons for the green valley galaxies to those discussed previously for the subset of red galaxies studied. For the red galaxies, an argument can be made for two possible tracks across the green valley, shown by the bimodal nature of both distributions in τ with a common area in the intermediate timescales region where the rapid and slow timescales peaked distributions intersect. However in the green valley this intermediate quenching timescale region becomes more significant (in agreement with the conclusions of Gonçalves et al. 2012), particularly for the smooth-like galaxies (see the left panel of Figure 3.3).

The smooth galaxy parameters favour these intermediate quenching timescales (40.6%) with some preference for slow quenching at early times ($z > 1$). The preference for rapid quenching of smooth galaxies has dropped by over a half compared to the red galaxies, however this will be influenced by the observability of galaxies undergoing such a rapid quench which will spend significantly less time in the transitional population of the green valley. Those galaxies with such a rapid decline in star formation will pass so quickly through the green valley they will be detected at a lower number than those galaxies which have stalled in the green valley with intermediate quenching timescales; accounting for the observed number of intermediate galaxies which are present in the green valley and the dominance of rapid timescales detected for red galaxies for both morphologies.

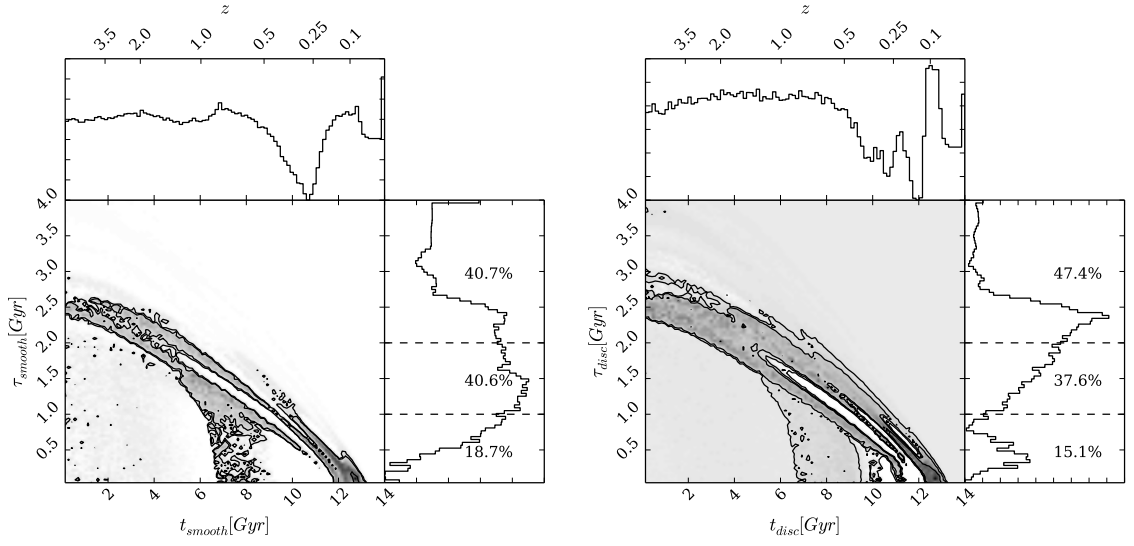


Figure 3.3: Contour plots showing the combined positions in the Markov Chain for galaxies in the green valley, weighted by the logarithmic probability of each position (see Section 2.2) and also by the morphological vote fractions from GZ2 to give the areas of high probability in the model parameter space for both bulge (left) and disc (right) dominated systems. The histograms show the projection into one dimension for each parameter. The dashed lines show the separation between rapid (τ [Gyr] < 1.0), intermediate (1.0 < τ [Gyr] < 2.0) and slow (τ [Gyr] > 2.0) quenching timescales with the fraction of the combined posterior probability distribution in each region shown (see Section 2.2).

The disc galaxies of the green valley now overwhelmingly prefer slow quenching timescales (47.4%) with a similar amount of intermediate quenching compared to the smooth galaxy parameters (37.6%; see Figure 3.3). There is still some preference for galaxies with a star formation history which results in a high current SFR, suggesting there are also some late-type galaxies that have just progressed from the blue cloud into the green valley.

If we compare Figure 3.3 to Figure 3.2 we can see quenching has occurred at later (more recent) cosmic times in the green valley at least for red galaxies for both morphological types. Therefore both morphologies are tracing the evolution of the red sequence, confirming that the green valley is indeed a transitional population between blue cloud and red sequence regardless of morphology. Currently as we observe the green valley, its main constituents are very slowly evolving disc-like galaxies along with intermediate- and smooth-like galaxies which pass across it with intermediate timescales within $\sim 1.0 - 1.5$ Gyr.

Given enough time ($t \sim 4 - 5$ Gyr), the disc galaxies will eventually fully pass through the green valley and make it out to the red sequence (the right panel of Figure 2.2 shows galaxies with $\tau > 1.0$ Gyr do not approach the red sequence within 3 Gyr post quench). This is most likely the origin of the ‘red spirals’.

If we consider then that the green valley is a transitional population, then we can expect that the ratio of smooth:disc galaxies that is currently observed in the green valley will evolve into the ratio observed for the red galaxies with NUV emission investigated. Table ?? shows the ratio of smooth : disc galaxies in the observed red sequence of the GZ2 sample is 62 : 38 whereas in the green valley it is 45 : 55. Making the very simple assumptions that this ratio does not change with redshift and that quenching is the only mechanism which causes a morphological transformation, we can infer that 31.2% of the disc-dominated galaxies currently residing in the green valley would have to undergo a morphological change to a bulge-dominated galaxy. We find that the fraction of the probability for green valley disc galaxies occupying the parameter space $\tau < 1.5$ Gyr is 29.4%, and therefore suggest that quenching mechanisms with these timescales are capable of destroying the disc-dominated nature of galaxies. This is most likely an overestimate of the mechanisms with timescales that can cause a morphological change because of the observability of those galaxies which undergo such a rapid quench; Martin et al. (2007) showed that after considering

the time spent in the green valley, the fraction of galaxies undergoing a rapid quench quadruples.

All of this evidence suggests that there are not just two routes for galaxies through the green valley as concluded by S14, but a continuum of quenching timescales which we can divide into three general regimes: rapid ($\tau < 1.0$ Gyr), intermediate ($1.0 < \tau < 2.0$ Gyr) and slow ($\tau > 2.0$ Gyr). The intermediate quenching timescales reside in the space between the extremes sampled by the UV/optical diagrams of S14; the inclusion of the intermediate galaxies in this investigation (unlike in S14) and the more precise Bayesian analysis, quantifies this range of τ and specifically ties the intermediate timescales to all variations of galaxy morphology.

3.3 Blue Cloud Galaxies

Since the blue cloud is considered to be primarily made of star forming galaxies we expect STARPY to have some difficulty in determining the most likely quenching model to describe them, as confirmed by Figure 3.4. The attempt to characterise a star forming galaxy with a quenched SFH model leads STARPY to attribute the extremely blue colours of the majority of these galaxies to fast quenching at recent times (i.e. very little change in the SFR; see the right panel of Figure 3.4 in comparison with the bottom panel of Figure 2.1).

This is particularly apparent for the blue disc population. Perhaps even galaxies which are currently quenching slowly across the blue cloud cannot be well fit by the quenching models implemented, as they still have high SFRs despite some quenching (although a galaxy has undergone quenching, star formation can still occur in a galaxy, just at a slower rate than at earlier times, described by τ).

There is a very small preference among blue bulge dominated galaxies for slow quenching which began prior to $z \sim 0.5$. These populations have been blue for a considerable period of time, slowly using up their gas for star formation by the Kennicutt–Schmidt law (Schmidt, 1959; Kennicutt, 1997). However the major preference is for rapid quenching at recent times in the blue cloud; this therefore provides some support to the theories for blue ellipticals as either merger-driven ($\sim 76\%$; like those identified as recently quenched ellipticals with properties consistent with a

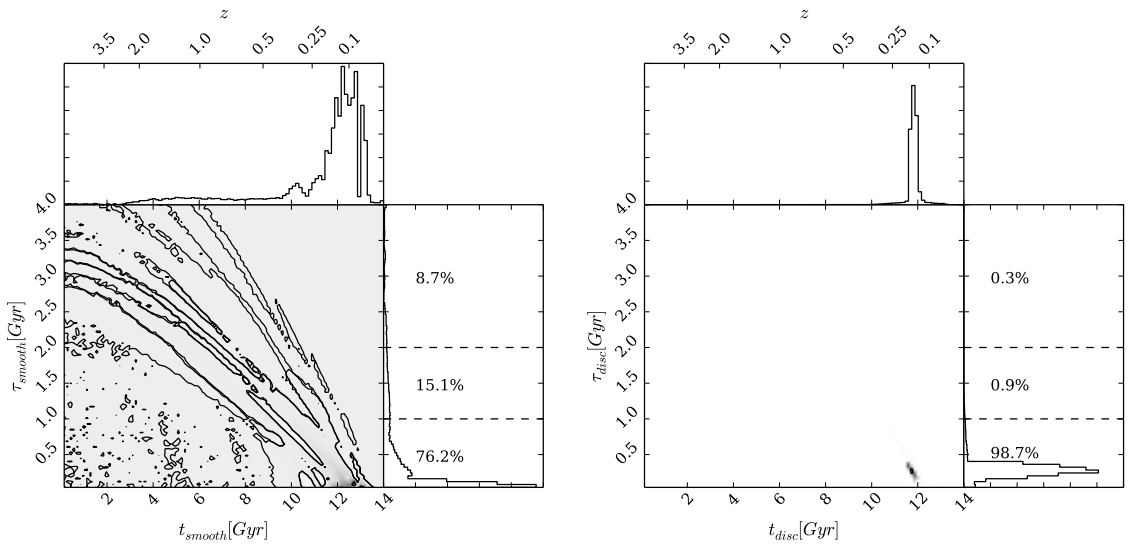


Figure 3.4: Contour plots showing the combined positions in the Markov Chain for galaxies in the blue cloud, weighted by the logarithmic probability of each position (see Section 2.2) and also by the morphological vote fractions from GZ2 to give the areas of high probability in the model parameter space for both bulge (left) and disc (right) dominated systems. The histograms show the projection into one dimension for each parameter. The dashed lines show the separation between rapid (τ [Gyr] < 1.0), intermediate ($1.0 < \tau$ [Gyr] < 2.0) and slow (τ [Gyr] > 2.0) quenching timescales with the fraction of the combined posterior probability distribution in each region shown (see Section 2.2). Positions with probabilities less than 0.2 are discarded as poorly fit models, therefore we can conclude unsurprisingly that blue cloud galaxies are not well described by a quenching star formation model.

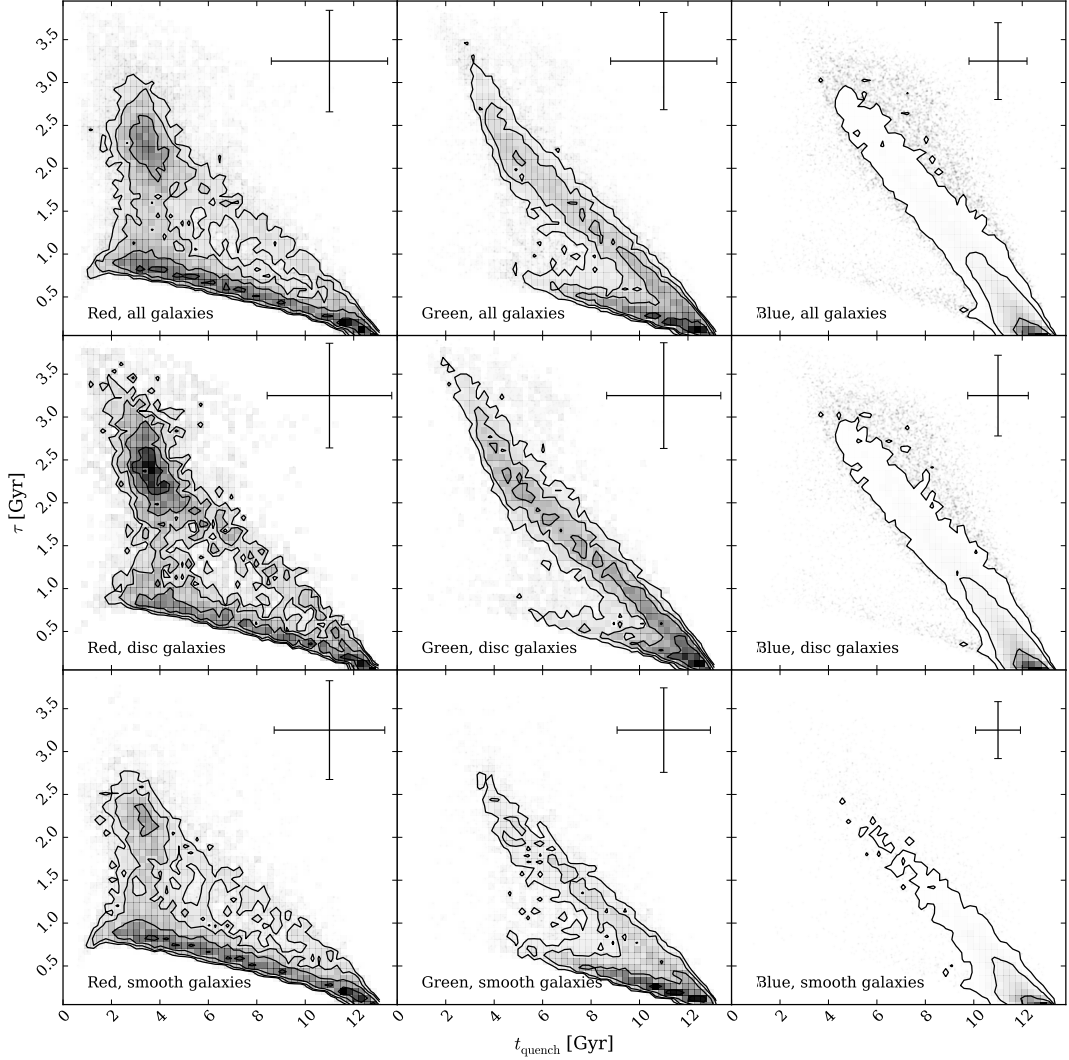


Figure 3.5: Contours showing the positions in the $[t, \tau]$ parameter space of the median walker position (the 50th percentile; as shown by the intersection of the solid blue lines in Figure 2.2) for each galaxy for all (top), disc ($p_d > 0.5$; middle), and smooth ($p_s > 0.5$; bottom) red sequence, green valley and blue cloud galaxies in the left, middle and right panels respectively. The error bars on each panel shows the average 68% confidence on the median positions (calculated from the 16th and 84th percentile, as shown by the blue dashed lines in Figure 2.2). These positions were calculated without discarding any walker positions due to low probability and without weighting by vote fractions, therefore this plot may be more intuitive than Figures 3.2, 3.3 & 3.4. The differences between the smooth and disc populations and between the red, green and blue populations remain clearly apparent.

merger origin by McIntosh et al. 2014) or gas inflow-driven reinvigorated star formation that is now slowly decreasing ($\sim 24\%$; such as the population of blue spheroidal galaxies studied by Kaviraj et al. 2013). However, we remind the reader that the quenching models used in this work do not provide an adequate fit to the blue cloud population.

The blue cloud is therefore primarily composed of both star forming galaxies with any morphology and smooth galaxies which are undergoing a rapid quench, presumably after a previous event triggered star formation and turned them blue.

Chapter 4

The Influence of AGN Feedback

The work in the following chapter has been published in Smethurst et al. (2016).

AGN can have a big impact on a galaxy.

4.0.1 Bulgeless galaxies hosting growing black holes

Chapter 5

The influence of the group environment

Mass quenching more important. Environment somewhat but not ram pressure stripping.

Chapter 6

Discussion

This is where I blow the lid of quenching. Bring it all together in a big happy family picture.

Chapter 7

Conlusions

Quenching is morphologically dependant.

AGN may be responsible for some of this quenching.

The environment plays less of a role than typical mass quenching.

Bibliography

- Arnouts S. et al., 2007, A&A, 476, 137
- Baldry I. K., Balogh M. L., Bower R. G., Glazebrook K., Nichol R. C., Bamford S. P., Budavari T., 2006, MNRAS, 373, 469
- Baldry I. K., Glazebrook K., Brinkmann J., Ivezić Ž., Lupton R. H., Nichol R. C., Szalay A. S., 2004, ApJ, 600, 681
- Ball N. M., Loveday J., Brunner R. J., 2008, MNRAS, 383, 907
- Bamford S. P. et al., 2009, MNRAS, 393, 1324
- Barro G. et al., 2013, ApJ, 765, 104
- Bell E. F. et al., 2004, ApJ, 608, 752
- Béthermin M. et al., 2012, ApJ, 757, L23
- Bower R. G., Benson A. J., Malbon R., Helly J. C., Frenk C. S., Baugh C. M., Cole S., Lacey C. G., 2006, MNRAS, 370, 645
- Bower R. G., Lucey J. R., Ellis R. S., 1992, MNRAS, 254, 601
- Brammer G. B. et al., 2009, ApJ, 706, L173
- Bruzual G., Charlot S., 2003, MNRAS, 344, 1000
- Canalizo G., Stockton A., 2001, ApJ, 555, 719
- Chabrier G., 2003, PASP, 115, 763
- Chen X. Y., Liang Y. C., Hammer F., Prugniel P., Zhong G. H., Rodrigues M., Zhao Y. H., Flores H., 2010, A&A, 515, A101

- Chester C., Roberts M. S., 1964, AJ, 69, 635
- Cheung E. et al., 2012, ApJ, 760, 131
- Coil A. L. et al., 2008, ApJ, 672, 153
- Conroy C., Gunn J. E., White M., 2009, ApJ, 699, 486
- Constantin A., Hoyle F., Vogeley M. S., 2008, ApJ, 673, 715
- Cowie L. L., Barger A. J., 2008, ApJ, 686, 72
- Croton D. J. et al., 2006, MNRAS, 365, 11
- Daddi E. et al., 2007, ApJ, 670, 156
- Daddi E. et al., 2010, ApJ, 714, L118
- Darg D. W. et al., 2010, MNRAS, 401, 1043
- De Lucia G., Tornatore L., Frenk C. S., Helmi A., Navarro J. F., White S. D. M., 2014, MNRAS, 445, 970
- Di Matteo T., Springel V., Hernquist L., 2005, Nature, 433, 604
- Dressler A., 1980, ApJ, 236, 351
- Driver S. P. et al., 2006, MNRAS, 368, 414
- Elbaz D. et al., 2007, A&A, 468, 33
- Eminian C., Kauffmann G., Charlot S., Wild V., Bruzual G., Rettura A., Loveday J., 2008, MNRAS, 384, 930
- Faber S. M. et al., 2007, ApJ, 665, 265
- Fabian A. C., 2012, ARA&A, 50, 455
- Falkenberg M. A., Kotulla R., Fritze U., 2009, MNRAS, 397, 1954
- Fang J. J., Faber S. M., Koo D. C., Dekel A., 2013, ApJ, 776, 63
- Foreman-Mackey D., Hogg D. W., Lang D., Goodman J., 2013, PASP, 125, 306
- Glazebrook K. et al., 2003, ApJ, 587, 55

- Gonçalves T. S., Martin D. C., Menéndez-Delmestre K., Wyder T. K., Koekemoer A., 2012, ApJ, 759, 67
- González V., Labbé I., Bouwens R. J., Illingworth G., Franx M., Kriek M., Brammer G. B., 2010, ApJ, 713, 115
- Goodman J., Weare J., 2010, CAMCS, 5, 65
- Häring N., Rix H.-W., 2004, ApJ, 604, L89
- Heinis S. et al., 2014, MNRAS, 437, 1268
- Hickox R. C. et al., 2009, ApJ, 696, 891
- Kaviraj S. et al., 2013, MNRAS, 428, 925
- Kennicutt R. C., 1997, in Astrophysics and Space Science Library, Vol. 161, Astrophysics and Space Science Library, pp. 171–195
- Kennicutt, Jr. R. C., Roettiger K. A., Keel W. C., van der Hulst J. M., Hummel E., 1987, AJ, 93, 1011
- Kriek M. et al., 2010, ApJ, 722, L64
- Lahav O., Bridle S. L., Hobson M. P., Lasenby A. N., Sodré L., 2000, MNRAS, 315, L45
- Lintott C. et al., 2011, MNRAS, 410, 166
- Lintott C. J. et al., 2009, MNRAS, 399, 129
- Mackay D. J. C., 2003, Information Theory, Inference and Learning Algorithms. p. 640
- Magorrian J. et al., 1998, AJ, 115, 2285
- Marasco A., Fraternali F., Binney J. J., 2012, MNRAS, 419, 1107
- Maraston C., 2005, MNRAS, 362, 799
- Marconi A., Hunt L. K., 2003, ApJ, 589, L21
- Martin D. C. et al., 2007, ApJS, 173, 342
- Masters K. L. et al., 2010, MNRAS, 405, 783

- Masters K. L. et al., 2011, MNRAS, 411, 2026
- McIntosh D. H. et al., 2014, MNRAS, 442, 533
- Melbourne J. et al., 2012, ApJ, 748, 47
- Mendez A. J., Coil A. L., Lotz J., Salim S., Moustakas J., Simard L., 2011, ApJ, 736, 110
- Miner J., Rose J. A., Cecil G., 2011, ApJ, 727, L15
- Nair P. B., Abraham R. G., 2010, ApJL, 714, L260L264
- Nandra K. et al., 2007, ApJ, 660, L11
- Noeske K. G. et al., 2007, ApJ, 660, L43
- Pan Z., Li J., Lin W., Wang J., Kong X., 2014, ApJ, 792, L4
- Peng C. Y., Ho L. C., Impey C. D., Rix H.-W., 2010, AJ, 139, 2097
- Peng Y.-j., Lilly S. J., Renzini A., Carollo M., 2012, ApJ, 757, 4
- Salim S. et al., 2007, ApJS, 173, 267
- Sánchez-Blázquez P., Gorgas J., Cardiel N., González J. J., 2006, A&A, 457, 809
- Schawinski K., Thomas D., Sarzi M., Maraston C., Kaviraj S., Joo S.-J., Yi S. K., Silk J., 2007, MNRAS, 382, 1415
- Schawinski K. et al., 2014, MNRAS, 440, 889
- Schawinski K. et al., 2010, ApJ, 711, 284
- Schawinski K., Virani S., Simmons B., Urry C. M., Treister E., Kaviraj S., Kushkuley B., 2009, ApJ, 692, L19
- Schiminovich D. et al., 2007, ApJS, 173, 315
- Schmidt M., 1959, ApJ, 129, 243
- Silk J., Rees M. J., 1998, A&A, 331, L1
- Sivia D., Skilling J., 2006, Data Analysis: A Bayesian Tutorial, Oxford science publications. OUP Oxford

- Skibba R. A. et al., 2009, MNRAS, 399, 966
- Smethurst R. J. et al., 2016, MNRAS
- Smethurst R. J. et al., 2015, MNRAS, 450, 435
- Somerville R. S., Hopkins P. F., Cox T. J., Robertson B. E., Hernquist L., 2008, MNRAS, 391, 481
- Strateva I. et al., 2001, AJ, 122, 1861
- Tojeiro R., Heavens A. F., Jimenez R., Panter B., 2007, MNRAS, 381, 1252
- Tojeiro R. et al., 2013, MNRAS, 432, 359
- Trager S. C., Faber S. M., Worthey G., González J. J., 2000, AJ, 120, 165
- Vazdekis A., Sánchez-Blázquez P., Falcón-Barroso J., Cenarro A. J., Beasley M. A., Cardiel N., Gorgas J., Peletier R. F., 2010, MNRAS, 404, 1639
- Willett K. W. et al., 2013, MNRAS, 435, 2835
- Willmer C. N. A. et al., 2006, ApJ, 647, 853
- Wyder T. K. et al., 2007, ApJS, 173, 293